Channel-like slippage modes in the human anion/proton exchanger ClC-4

Alexi K. Alekov[1] and Christoph Fahlke[1,2]

[1]Institut für Neurophysiologie, Medizinische Hochschule Hannover, 30625 Hannover, Germany
[2]Zentrum für Systemische Neurowissenschaften Hannover, 30559 Hannover, Germany

The ClC family encompasses two classes of proteins with distinct transport functions: anion channels and transporters. ClC-type transporters usually mediate secondary active anion–proton exchange. However, under certain conditions they assume slippage mode behavior in which proton and anion transport are uncoupled, resulting in passive anion fluxes without associated proton movements. Here, we use patch clamp and intracellular pH recordings on transfected mammalian cells to characterize exchanger and slippage modes of human ClC-4, a member of the ClC transporter branch. We found that the two transport modes differ in transport mechanisms and transport rates. Nonstationary noise analysis revealed a unitary transport rate of 5×10^5 s^{-1} at +150 mV for the slippage mode, indicating that ClC-4 functions as channel in this mode. In the exchanger mode, unitary transport rates were 10-fold lower. Both ClC-4 transport modes exhibit voltage-dependent gating, indicating that there are active and non-active states for the exchanger as well as for the slippage mode. ClC-4 can assume both transport modes under all tested conditions, with exchanger/channel ratios determined by the external anion. We propose that binding of transported anions to non-active states causes transition from slippage into exchanger mode. Binding and unbinding of anions is very rapid, and slower transitions of liganded and non-liganded states into active conformations result in a stable distribution between the two transport modes. The proposed mechanism results in anion-dependent conversion of ClC-type exchanger into an anion channel with typical attributes of ClC anion channels.

The Journal of General Physiology

INTRODUCTION

Channels and carriers transport ions across the membrane using distinct transport mechanisms. Whereas channels mediate passive diffusion through aqueous pores, coupled transport by carriers is believed to occur by an aqueous conduction pathway with two gates that never open simultaneously, but allow alternating access to the external and the internal medium (Jardetzky, 1966). Members of a large family of anion transport proteins, the ClC family, were generally assumed to function as anion channels until reconstituted ClC-ec1 from *Escherichia coli* was shown to mediate secondary-active coupled antiport of anions and protons (Accardi and Miller, 2004). Subsequently, mammalian and plant ClC isoforms were also recognized to function as transporters (Picollo and Pusch, 2005; Scheel et al., 2005; De Angeli et al., 2006; Graves et al., 2008; Matsuda et al., 2008). The existence of different functional subclasses within the ClC family demonstrated the similarity of transporters and channels in this class of proteins and raised the question as to the molecular determinants that define ClC channels or transporters.

In the presence of certain anions, ClC exchangers assume a so-called slippage mode; i.e., they mediate a passive anion transport without thermodynamically coupled proton flux (Accardi et al., 2005, 2006; Nguitragool and Miller, 2006; Walden et al., 2007; Zdebik et al., 2008). At present, little is known about the function of ClC exchangers in the slippage mode. The slippage mode might be characterized by passive anion diffusion through aqueous pores in a channel-mediated fashion, or it could involve larger conformational changes following a uniporter function.

Here, we examined slippage mode behavior of a member of the ClC transporter branch, human ClC-4. ClC-4 is localized in intracellular membranes of the brain, muscle, and liver. When heterologously expressed in mammalian cells, ClC-4 also inserts into the surface membrane, allowing separate measurement of anion and proton transport by simultaneous patch clamp and intracellular pH recordings. Using anion exchange experiments and noise analysis, we demonstrate that ClC-4 can switch from coupled to an uncoupled slippage mode of operation that has all the properties of channel-like anion conduction.

Correspondence to Christoph Fahlke: fahlke.christoph@mh-hannover.de

The Rockefeller University Press $30.00
J. Gen. Physiol. Vol. 133 No. 5 485–496
www.jgp.org/cgi/doi/10.1085/jgp.200810155

MATERIALS AND METHODS

Cell culture

HEK293 cell lines stably expressing ClC-4 (Hebeisen et al., 2003) were cultured in standard MEM medium, supplemented with 10% FBS and 900 µg/ml geneticin (G418; Invitrogen). Two different oligoclonal cell lines with indistinguishable functional characteristics of hClC-4 were used. Endogenous anion currents in nontransfected HEK293 cells were much smaller than those in stably transfected cells (in external SCN^- at +145 mV: untransfected cells: 0.59 ± 0.05 nA; $n = 10$; transfected cells: 7.0 ± 0.6 nA; $n = 26$). Moreover, under all tested ionic conditions, endogenous anion currents in nontransfected HEK293 cells were not associated with proton currents.

Electrophysiology

Standard whole cell patch clamp (Hamill et al., 1981) was performed using an EPC-10 amplifier controlled by PatchMaster acquisition software (HEKA). Borosilicate pipettes were pulled with resistances of 1–5 MΩ. Capacitive cancellation and series resistance compensation were applied to reduce capacitive artifacts and series resistance errors, resulting in voltage errors <5 mV. Currents were digitized with 10–100-kHz sampling rates after analogue filtering with less than one third of the sampling frequency. Junction potentials were corrected a posteriori using the JPCalc software (Barry, 1994). The composition of the standard solutions was (in mM): 140 extracellular NaCl, 4 KCl, 2 $CaCl_2$, 1 $MgCl_2$, and 5 HEPES, pH 7.0, and 105 intracellular NaCl, 5 $MgCl_2$, 5 Na_2ATP, 5 EGTA, and 1 HEPES, pH 7.0. For experiments not including fluorescence pH detection, HEPES concentration in the pipette solution was increased to 10 mM (and NaCl concentration reduced to 96 mM to preserve osmolarity). In some of the experiments, external and/or internal Cl^- was substituted partially with SCN^-, NO_3^-, I^-, Br^-, F^-, or gluconate on an equimolar basis. For all experiments, we used external and/or internal agar salt bridges made from plastic tubing filled with 3 M KCl in 0.8% agar to connect the Ag/AgCl electrodes to the bath/pipette solution.

Measurements of intracellular pH and relative proton flux

For experiments measuring ClC-4–mediated proton transport, cells were cultivated on collagen-coated glass coverslips and mounted in a perfusion chamber on an inverted IX71 microscope with a UPlanSApo 60X/1.35 oil-immersion objective (Olympus). The pH-sensitive dye 2',7'-bis-(2-carboxyethyl)-5-(and-6)-carboxyfluorescein (BCECF; Invitrogen) was loaded at a concentration of 150 µM through the pipette. The loading procedure was monitored by measuring the time course of fluorescence intensity increase after establishing the whole cell mode. Electrophysiological recordings were not started before complete equilibration between pipette and cytoplasm (3–5 min). The dye was excited sequentially at 440 and 490 nm using a Polychrome V fast-switching monochromator, and emitted fluorescence light was detected at 530 nm using a PMT-equipped ViewFinder III (Till Photonics). Fluorescence excitation and detection were software controlled by the photometry extension of PatchMaster. F490/F440 ratios were calculated and converted into absolute pHs after a background fluorescence correction. BCECF had equal pH response when dissolved in the pipette solution or in intact HEK cells loaded with the AM ester (Fig. S1 A). Proton fluxes were estimated as the rates of intracellular pH changes ($\Delta pH/\Delta t$).

Measurements of absolute proton fluxes

Absolute proton fluxes ($\phi_{H^+} = \beta V \Delta pH / \Delta t$) and proton currents ($I_{H^+} = F\Phi_{H^+}$, with F being the Faraday constant) were calculated from the rates of intracellular pH changes ($\Delta pH/\Delta t$) using the volume (V) and the specific buffering capacity (β) of the particular cell. In these experiments, sodium was substituted by tetramethylammonium to minimize the effects of endogenous sodium/proton exchangers. Moreover, cells were incubated for 60 min before recording with 100 nM bafilomycin to block possible proton pump activity in HEK293 cells (Lang et al., 2003).

Volume and buffering capacity were individually measured at the end of each experiment. Before establishing whole cell configuration, cells were detached from the surface to achieve a semispherical form of the studied cell. For calculating cell volume, the longest and the shortest two-dimensional geometrical measure of each cell were measured using video microscopy. Buffering capacity was measured individually in each cell at the end of the experiments using the ammonium jump technique by applying and washing out solutions containing 30 mM NH_4Cl (Fig. S1 B) (Roos and Boron, 1981).

At the end of each experiment, cells were clamped at 0 mV, and the time course of intracellular pH recovery was determined (Fig. S1 C). Because patch access resistances are at least two orders of magnitude lower than whole cell seal resistances, pH equilibration is dominated by proton delivery through the patch pipette and can be modeled as diffusion process with $\Delta pH_{RECOVERY}/\Delta t = -D\left(pH_{INTRACELLULAR} - pH_{PIPETTE}\right)$ (Mathias et al., 1990). We used pHs instead of proton concentrations ($[H^+]$) because of the proportionality $\Delta[H^+] = \beta\Delta pH$, with β being the proton-buffering capacity. The time course of pH changes followed a monoexponential time course (Fig. S1 C), and diffusion coefficients were determined as the inverse time constant ($D = 1/\tau$). Subsequently, the corrected pH was calculated stepwise from $\Delta pH_{CORR} = \Delta pH_{MEASURED} - \Delta pH_{RECOVERY}$, and the corrected rate of pH change $\Delta pH_{CORR} / \Delta t$ was obtained.

Noise analysis

For nonstationary noise analysis, currents were digitized at 100 kHz after filtering with a 15-kHz Butterworth filter. Series of 300–600 current responses to 150-mV voltage steps were recorded and analyzed using PulseTools (HEKA) using the procedures described elsewhere (Heinemann and Conti, 1992). Variances were binned, and statistical errors were superimposed as error bars. For further analysis, the background noise was determined as the variance at zero current and subtracted. To obtain the unitary properties of the process, background-corrected variances σ^2 or ratios σ^2/I of variance by the mean current I were plotted against I. Unitary current amplitude i and number of ClC-4 proteins N were then obtained by fitting the parabolic function

$$\sigma^2 = iI - \frac{I^2}{N}$$

or a linear function

$$\frac{\sigma^2}{I} = i - \frac{I}{N}$$

to the data (Sigworth, 1980). Power spectrum analysis was performed on the steady-state phase of 500-ms long pulses to different potentials using FitMaster and fitted with a double Lorentzian function,

$$S = \frac{S(0)_1}{1 + f/fc_1} + \frac{S(0)_2}{1 + f/fc_2},$$

where S and f denote the spectral density and the frequency, $S(0)_{1/2}$ and $fc_{1/2}$ are the amplitudes and corner frequencies of the correspondent Lorentzian term.

Single-channel simulation

Single-channel simulation was performed with the QuB software package (version 1.4.0.121; http://www.qub.buffalo.edu) in its standard configuration. Simulations were performed modeling a simple closed ↔ open gating diagram

$$(C \underset{K_{off}}{\overset{K_{on}}{\leftrightarrow}} O)$$

using the standard program settings. Channels were simulated with an open probability of 0.5 (as determined by nonstationary noise analysis for ClC-4; Fig. 3). The duration of the mean open lifetimes was varied by the closing rate constant K_{off}. In all simulations the single-channel amplitude was set to 1.

Data analysis

Data were analyzed with a combination of FitMaster, PulseTools (HEKA), Origin 6 (OriginLab Corporation), and Excel (Microsoft Corporation) programs. Kinetic simulations were performed using Matlab 6 (The MathWorks, Inc.). Dependence of the ClC-4 current amplitude I on the anion concentration $[A^-]$ was fitted with a standard binding curve with a Hill coefficient of 1,

$$I = \frac{I_{\max}[A^-]}{K_M + [A^-]},$$

$I_{\max}$ and K_M denote the maximal saturation value of the current and the apparent Michaelis constant, respectively. All summary values are shown as mean ± SEM.

Online supplemental material

Fig. S1 shows the calibration procedure for measuring intracellular pH with BCECF and the procedures for determining intracellular buffering constants and for correcting proton flux data bias caused by the exchange between cell interior and pipette solution. Fig. S2 illustrates ClC-4–mediated anion and proton currents in cells dialyzed with a NO_3^--based pipette solution. Fig. S3 demonstrates the voltage dependence of ClC-4 gating. Fig. S4 depicts a simulation of a model proposed by us to explain the effects of extracellular anions on ClC-4 transport properties. It is accompanied by supplemental text. Fig. S5 provides additional information about the design of the experiments used to demonstrate time-dependent changes in ClC-4 proton transport. Figs. S1–S5 are available at http://www.jgp.org/cgi/content/full/jgp.200810155/DC1.

RESULTS

Human ClC-4 mediates anion/proton exchange with variable stoichiometry

We combined patch clamp recordings and fluorescence measurements of intracellular pH in mammalian cells stably expressing ClC-4 (Fig. 1). Proton fluxes were determined as rates of intracellular pH change ($\Delta pH/\Delta t$), and whole cell currents were measured in parallel. Total currents and proton fluxes are minimal at negative potentials but increase with depolarization, resulting in a pronounced outward rectification (Fig. 1, A and B).

Substitution of external Cl^- with other permeant anions modifies both total currents and proton fluxes. Fig. 1 (C and D) gives voltage dependences of proton fluxes and whole cell current amplitudes measured at the end of 50-ms voltage steps. For comparison, currents and fluxes were normalized to corresponding values determined in external Cl^- at the same cell. NO_3^- and SCN^- increase maximum current amplitudes (Fig. 1 C) but decrease proton fluxes (Fig. 1 D). In contrast, Br^- and I^- block current amplitudes as well as proton fluxes (Fig. 1, C and D). F^- is a potent ClC-4 blocker, reducing

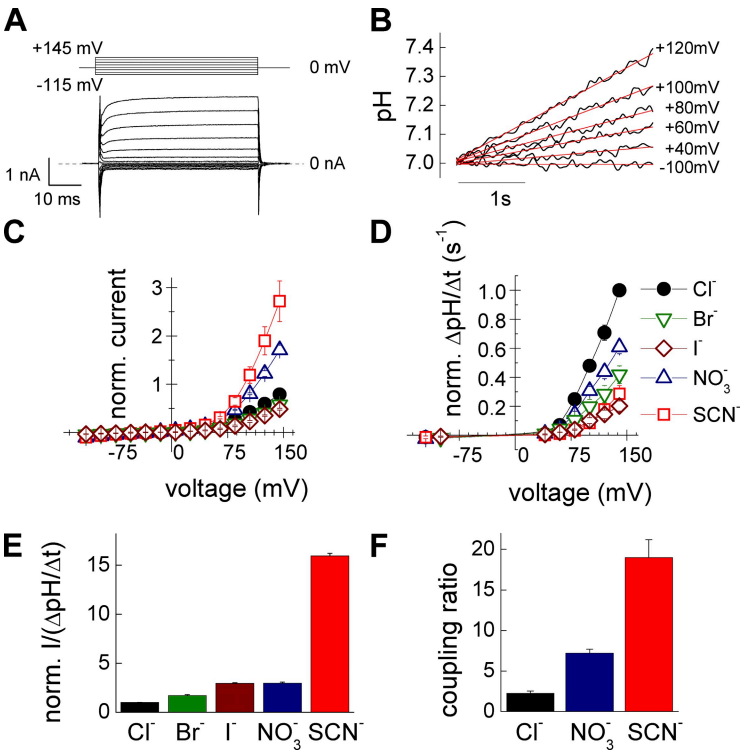

Figure 1. External anions modify the anion/proton transport stoichiometry. (A) Pulse protocol and representative ClC-4 whole cell current traces in standard Cl^--based intracellular and extracellular solutions. (B) Time courses of intracellular pH changes at the same cell at various test potentials. Red lines show linear fits to obtain $\Delta pH/\Delta t$. (C) Current–voltage dependences measured for various external anions with Cl^- intracellular solution. Cells were sequentially perfused with different extracellular anions, and current amplitudes were normalized to currents determined in Cl^--based external solution ($n = 4$–6). (D) Rates of intracellular pH change in the same cells as in C normalized to values obtained in Cl^--based external solution. (E) Relative current to proton flux ratio for Cl^-, Br^-, I^-, NO_3^-, and SCN^- at +90 mV. (F) Absolute anion to proton transport stoichiometry for Cl^-, NO_3^-, and SCN^- determined at +90 mV ($n = 4$–7).

whole cell currents to background levels and completely depressing proton flux (not depicted). Under all tested anion compositions, ratios of measured total current by the rate of intracellular pH variation did not change with voltage between +60 and +140 mV. Because proton currents are proportional to intracellular pH changes, we conclude that anion and proton transport rates exhibit similar voltage dependences.

We next calculated relative anion–proton transport stoichiometries by dividing ionic currents by the rate of intracellular acidification and normalizing these values to the ratio obtained at the same cell in extracellular Cl^- (Fig. 1 E). Depending on the external anion, the transport ratio increased in an order of $Cl^- < Br^- < I^- \sim NO_3^- < SCN^-$. Larger and polyatomic anions thus increase the number of anions passing through the membrane per transported proton. We performed these experiments with Cl^--based pipette solution, but similar results were also obtained with intracellular NO_3^- (Fig. S2).

For three anions, Cl^-, NO_3^-, and SCN^-, we determined ratios of absolute anion/H^+ transport rates (Fig. 1 F). These measurements were performed with symmetrical anion compositions. Proton currents were calculated from changes of the intracellular pH using volume (V) and specific buffering capacities (β) of individual cells (see Materials and methods) (Roos and Boron, 1981). Transport stoichiometries calculated from total current (I_{tot}) and proton current amplitudes (I_{prot}) as $(I_{tot} - I_{prot})/I_{prot}$ were 2.2 ± 0.3 (n = 7) for Cl^-, 7.2 ± 0.5 (n = 5) for NO_3^-, and 18.9 ± 2.4 (n = 4) for SCN^- (Fig. 1 F). Due to the limitations in measurements of absolute proton fluxes (see Discussion), these values represent only lower limits of the transport stoichiometry.

The apparent transport stoichiometries observed for NO_3^- and SCN^- largely exceed values usually observed in coupled transporters and thus argue against a gradual change in the transport stoichiometry of a thermodynamically coupled anion–proton exchanger. However, this result is well explained by the coexistence of two transport modes; i.e., an exchanger mode in which ClC-4 functions as a thermodynamically coupled anion–proton exchanger and a slippage mode with anions slipping through the protein without associated proton movements.

Anion–protein interactions determine the transport mode of ClC-4

We next recorded ClC-4 currents in mixtures of the two anions with the most different coupling ratios, Cl^- and SCN^-. Increasing external [Cl^-] at constant $[SCN^-]_{out}$ reduced current amplitudes but augmented proton fluxes (Fig. 2, A and B). Plotting current amplitudes and proton fluxes against the Cl^- concentration reveals a nonlinear saturating dependence (Fig. 2 C), indicating that a rate-limiting binding step in the interaction between ClC-4 protein and transported anion defines transmembrane transport rates. Ionic currents decrease and proton fluxes increase with the same Cl^- concentration dependence (apparent Michaelis constant K_M: 25 ± 3 mM for the concentration dependence of total currents, and 28 ± 5 mM for proton currents; n = 4–5). The Cl^- dependence of current and proton fluxes was different when determined in experiments performed in the absence of thiocyanate (Fig. 6 B) or in the presence of 100 mM SCN^- (not depicted), suggesting a binding competition between Cl^- and SCN^-. We conclude that binding of Cl^- ions to a specific site favors the coupled anion/proton exchanger function of ClC-4 (Fig. 2 C). Cl^- acts as blocker of SCN^- currents but as agonist for anion/proton exchange.

The number of all ClC-4 proteins in the cell membrane is expected to be constant during anion exchange

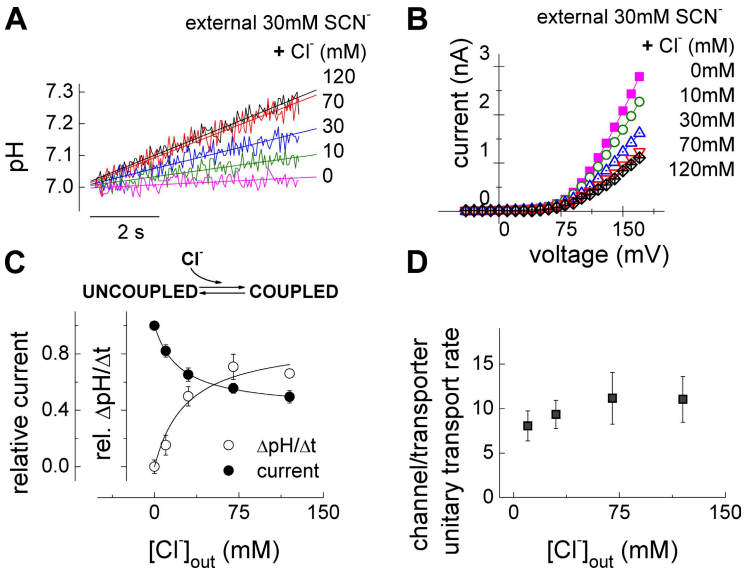

Figure 2. External Cl^- promotes coupled anion–proton exchange. (A) Representative intracellular pH time course at +90 mV in a ClC-4 expressing cell perfused with extracellular solutions containing 30 mM SCN^- and variable concentrations of Cl^-. Solid lines represent linear fits. (B) Normalized current–voltage relationships from the same cell at extracellular solutions containing 30 mM SCN^- and variable concentrations of Cl^-. (C) Variation of normalized current amplitudes and normalized proton fluxes by increasing concentrations of Cl^- at +90 mV (n = 4–5). Lines represent fits with standard one-site binding function (Michaelis-Menten functions). (D) Ratios of unitary transport rates of H^+-coupled and uncoupled ClC-4 currents for different [Cl^-] with constant [SCN^-] at +90 mV (n = 3).

experiments. Changes in the total current (ΔI) and in the proton current amplitude ($\Delta I_p = \beta VF(\Delta pH / \Delta t)$; see Materials and methods) thus depend on the individual transport rates of the corresponding modes as well as on the number of ClC-4 proteins converted from one functional state to the other. Dividing changes of total current by changes of proton current amplitude ($\Delta I/\Delta I_p$) provides the ratio of the unitary current amplitude in the slippage mode by the unitary proton transport rate in the exchanger mode. We assumed that ClC-4 exhibits the same two anions to one proton transport stoichiometry as ClC-ec1 (Nguitragool and Miller, 2006) and ClC-7 (Graves et al., 2008), resulting in three transported charges per cycle in the coupled transporter mode. To obtain ratios of ion transport rates we therefore divided $\Delta I/\Delta I_p$ by three (Fig. 2 D; saturating value 11.0 ± 2.6; $n = 3$).

SCN^- transport resembles permeation through an aqueous pore

Noise analysis of macroscopic currents provides information about underlying unitary events and thus allows distinction of different transport processes (Verveen and DeFelice, 1974; Starace and Bezanilla, 2004). Whereas ion conduction through aqueous pores results in power spectra with Lorentzian shape, transporter mechanisms generate power spectra that rise and level off at high frequencies (Stevens, 1972; Kolb and Läuger, 1978). We first performed noise analysis with SCN^- as main external anion; i.e., under the ionic condition that results in a maximal number of ClC-4 in the slippage mode (Fig. 3). ClC-4 current power spectra can be well fit with a second-order Lorentzian function with corner frequencies of 32 and 1,270 Hz (Fig. 3 A). Corner frequencies f_c are predicted to reflect macroscopic current relaxation time constants τ_m by the relation $f_c = 1/(2\pi\tau_m)$. The corner frequency of 32 Hz at +135 mV is in good agreement with the activation time constant of ClC-4 macroscopic currents (6.6 ± 0.2 ms; $n = 9$). Under the same conditions, untransfected HEK cells showed lower current variances and power spectra resembling white 1/f noise (Fig. 3 A). In external Cl^-, whole cell ClC-4 currents exhibit noise with power spectral density one order of magnitude lower than in external SCN^- (not depicted).

We calculated upper limits for the spectral density of transporter-mediated shot noise using Schottky's theorem (S(f) = 2Iq, with I being the macroscopic current and q the net transported charge per shot; DeFelice, 1981). Predicted values of shot noise are much smaller than experimentally determined spectral densities for ClC-4 in external SCN^--based solution (experimental value for the cell in Fig. 3 A; S(48 Hz) = 1.4×10^{-25} A^2/Hz as compared with 2.8×10^{-27} A^2/Hz predicted for two anion/one proton exchangers or 9.6×10^{-28} A^2/Hz for uniporters).

These results indicate that, in external SCN^-, current variances in cells expressing ClC-4 represent Lorentzian noise arising from random on and off switching of unitary ClC-4 current events. This type of noise permits the application of nonstationary noise analysis to determine the amplitudes of the aforementioned events (Sigworth, 1980; Heinemann and Conti, 1992). We performed this analysis using an intracellular and extracellular solution containing I^- and SCN^- as predominant anions, respectively. I^- slows the time course of activation (Hebeisen et al., 2003) and provides ideal conditions for this analysis (Fig. 3, B and C). Current–variance plots could be fit with a parabolic function yielding a unitary current amplitude of 85 ± 8 fA ($n = 6$) at +150 mV (Fig. 3 C; see Materials and methods). A linear transformation ($\sigma^2 / I = i - I / N$) of the data in A) provides a more intuitive presentation of the results with the y-axis intercept providing the single-channel amplitude (Fig. 3 C, bottom). We repeated these experiments with Cl^- as main internal anion and obtained similar results (not depicted).

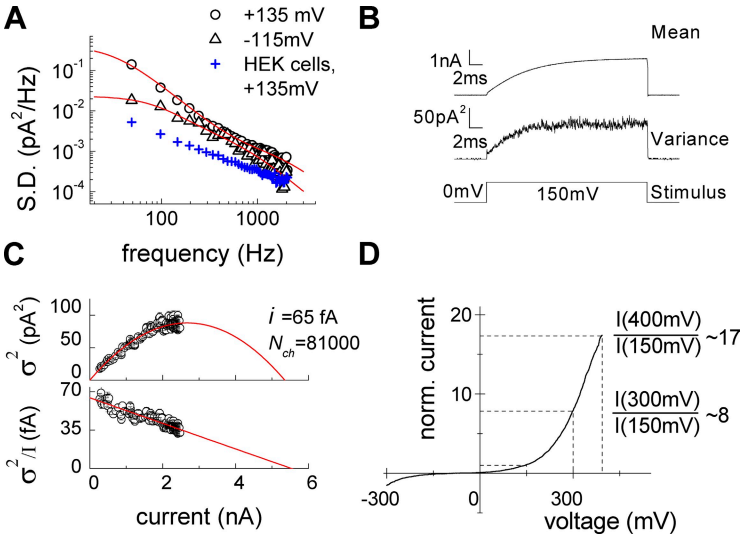

Figure 3. Unitary properties of ClC-4 in intracellular I^- and extracellular SCN^-. (A) Averaged power spectrum of ClC-4 currents from 30 sweeps after correction for background noise at −115 or +135 mV. Lines represent fits with a second-order Lorentzian function. Blue crosses depict a representative power spectrum from a nontransfected HEK293 cell in extracellular SCN^-. (B) Representative time course of ClC-4 mean currents and variances used for nonstationary noise analysis. (C) Current–variance plot (top panel) and linear transformation of the data (bottom panel) for the cell given in B. Red lines represent the fit with standard parabolic function (top panel) or a linear fit (bottom panel). (D) Representative ClC-4 current responses to a voltage ramp between −300 and +400 mV. Current amplitudes were normalized to the value at +150 mV.

Noise analysis demonstrates that the time and voltage dependence of macroscopic currents is caused by changes of the number of open channels upon voltage steps (Fig. 3). Moreover, it provides insights into the transport mechanisms of ClC-4 in the slippage mode. The calculated unitary current amplitude corresponds to $\sim 5 \times 10^5$ transported ions per second. Unitary transport rates for ClC-4 in the slippage mode are an order of magnitude higher than the highest transport rates reported for carriers; i.e., 5×10^4 for Cl^-/Cl^- exchange in the erythrocyte anion exchange transporter, AE1 (Brahm, 1977; Hille, 2001). A high unitary transport rate is a clear evidence for channel-mediated ion conduction (Hille, 2001) and suggests that ClC-4 functions as channel in its slippage mode. Because the unitary rate of coupled transport is 10 times smaller (Fig. 2 D), we calculated a value of 5×10^4 transported ions per second or of $\sim 2 \times 10^4$ transport cycles per second for the antiporter mode.

The pronounced rectification of ClC-4 provides an additional test for a channel-mediated transport in the slippage mode. If large conformational changes of the protein were associated with SCN^- transport, the transport rate should saturate at a certain value and not further increase, even at augmented electrochemical gradients upon further depolarization. In contrast, larger transport rates are possible when anions diffuse through aqueous pores. Upon ramp-like protocols with voltages that increase linearly with time, whole cell ClC-4 currents did not saturate up to +400 mV. Current amplitudes at +300 and +400 mV increased to values that are 8 and 17 times larger than the current amplitude at +150 mV (Fig. 3 D). Because ClC-4 activation curves measured under these conditions saturate at +180 mV (Fig. S3), this increase is entirely due to altered unitary current amplitudes: 0.7 pA at +300 mV and 1.4 pA at +400 mV. The values correspond to $\sim 5 \times 10^6$ and 10^7 transported ions per second and are comparable with single-channel amplitudes in ClC-1 and ClC-2 (Jentsch, 2008).

To estimate the duration of the unitary events underlying ClC-4 current noise, we investigated how filtering frequency affects current variances (Fig. 4) (Silberberg and Magleby, 1993). Decreasing low-pass filter cutoff frequency in the range of the single event duration will progressively affect the detected amplitude of the event (Fig. 4 A). We simulated single-channel activity of channels with one open and one closed state for various mean open life times and studied the effects of filtering on these simulated currents (Fig. 4 B). Fig. 4 C gives the dependence of the normalized standard deviation of simulated microscopic currents on the filter frequency for unitary events with different mean open durations. The normalized standard deviation ($SD = i\sqrt{Np(1-p)}$) is a measure of the unitary current amplitude, and Fig. 4 C thus provides the effect of the filter frequency on apparent single-channel current amplitudes determined by noise analysis. Our simulations demonstrate that ion channel recordings with a mean open time of 1 ms are only mildly affected by low-pass filtering between 1 and 15 kHz. Flickering channel activity (simulated here with the mean open time of 100 µs) will show pronounced effects of filtering at low frequencies but only minor changes at

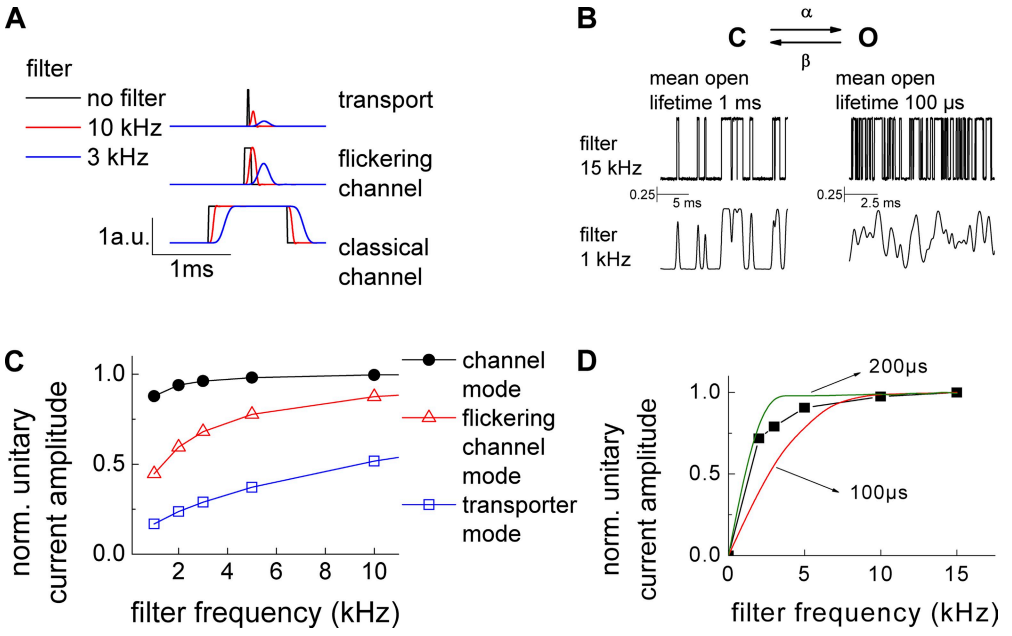

Figure 4. Effects of filtering on ClC-4 current noise. (A) Effects of low-pass filtering (3 and 10 kHz) on the amplitude of simulated single channels with different lengths: 10 µs (mimicking transporter mode), 100 µs (flickering ion channel), and 1 ms (ion channel). (B) Simulated single-channel events with 50% open probability and different mean open lifetimes (1 ms and 100 µs) before and after low-pass filtering with 1-kHz cutoff frequency. (C) Predicted effects of the low-pass filter frequency on the standard deviation of simulated single-channel traces with mean open lifetimes of 10 µs, 100 µs, and 1 ms. (D) Dependence of experimentally determined ClC-4 unitary current amplitude on the low-pass filter cutoff frequency. Nonstationary noise analysis was performed after offline filtering of macroscopic ClC-4 currents. The effects of low-pass filtering on simulated unitary events of 100 and 200 µs are given as solid lines.

high frequencies. In contrast, alternating access transporters likely generate shot noise with unitary events that correspond to δ functions (approximated by 10-µs mean lifetime durations in Fig. 4) and is reduced by filtering in an almost linear fashion (Galli et al., 1997). Fig. 4 D shows unitary current amplitudes obtained by noise analysis of ClC-4 macroscopic currents for different filtering frequencies in internal I^- and external SCN^- solution. Calculated unitary current amplitudes are modified by filtering as simulated single events with durations between 100 and 200 µs.

Cl^- binding reduces the apparent number of channels

Depending on rate constants of binding and unbinding, different ion channel blockers affect single-channel conductances, open probabilities, and the number of detected channels in a distinct way (Hille, 2001). Because Cl^- ions act as blocker of SCN^- currents through ClC-4, we used such analysis to study the kinetics of Cl^- binding to ClC-4. Fig. 5 shows the results of noise analysis from a single cell consecutively perfused with external solutions containing predominantly SCN^- as permeant anion (148 mM) and after substituting 75 mM SCN^- with 75 mM $gluconate^-$ or 75 mM Cl^-. Plots of the current variance versus the current amplitude or noise/current ratio versus current amplitude plots demonstrate that the unitary current amplitude is virtually unaltered by the addition of external Cl^- (Fig. 5 B, see initial slope of the parabolic fits; Fig. 5 C, see y-axis intercept of the linear fit to the noise/current ratio versus current amplitude ($\sigma^2 / I = i - I / N$)). In seven paired experiments, the addition of 75 mM Cl^- to 73 mM SCN^- significantly reduces the detected number of channels to 66 ± 6% (n = 7; P = 0.0016). In contrast, single-channel amplitude and maximum open probability were not affected by Cl^-. Substitution of SCN^- by $gluconate^-$ causes a reduction of the unitary current amplitude (Fig. 5, B and C), indicating that our measurements can accurately resolve single-channel variations.

Two different mechanisms of block are in agreement with such behavior. Cl^- might tightly bind to ClC-4 for time periods that exceed the duration of the voltage step (50 ms). We discarded this possibility because of the high transport rates in both modes. An alternative scenario is reminiscent of the gating model introduced to describe fast gating of ClC-0 (Chen and Miller, 1996). Our results demonstrated that ClC-4 can exist in two transport modes (Figs. 3 and 5), and that binding of the anion to a binding site in the protein causes the transition from the slippage into the exchanger mode (Figs. 2 and 5). Moreover, ClC-4–mediated anion currents are time and voltage dependent, indicating that there are at least one open and one closed state in the slippage mode. All of these features suggest the following state model:

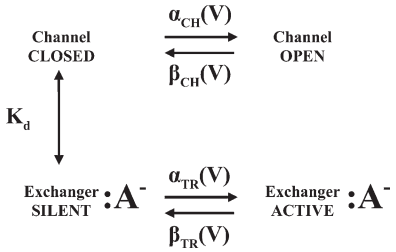

(SCHEME 1)

If the rate constants of anion binding are much faster than the opening transition of the channel, the proportions of ClC-4 without or with bound Cl^- will equilibrate into semi-equilibrium distribution. As a proof of principle, we simulated the effects of external [Cl^-] variation on the behavior of Scheme 1 and showed that fast binding and unbinding of anions to the nonconducting states predict the experimentally observed reduction in the number of channels by external Cl^- (Supplemental text and Fig. S4).

This scheme predicts that ClC-4 functions as a coupled transporter if a certain anion binding site is occupied. It also predicts that anion substitution will modify the number of ClC-4 functioning in the slippage or exchanger

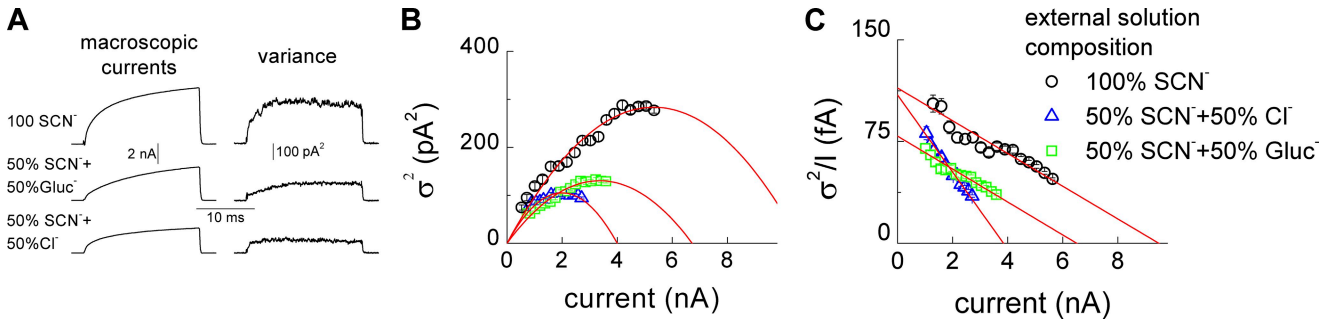

Figure 5. Cl^- reduces the number of channels detected by noise analysis. (A) Representative whole cell currents and current variances obtained in a cell stably expressing ClC-4 sequentially perfused with extracellular solution containing 100% SCN^-, 50% SCN^- plus 50% gluconate, and 50% SCN^- plus 50% Cl^-. An intracellular I^--based solution was used. (B) Current–variance plots of the data in A. Lines represent fits with standard parabolic function. (C) Linear transformation of the data in B. Note the different slope resulting when 50% of SCN^- anions were substituted with 50% Cl^- or gluconate. Lines represent linear fits to the data.

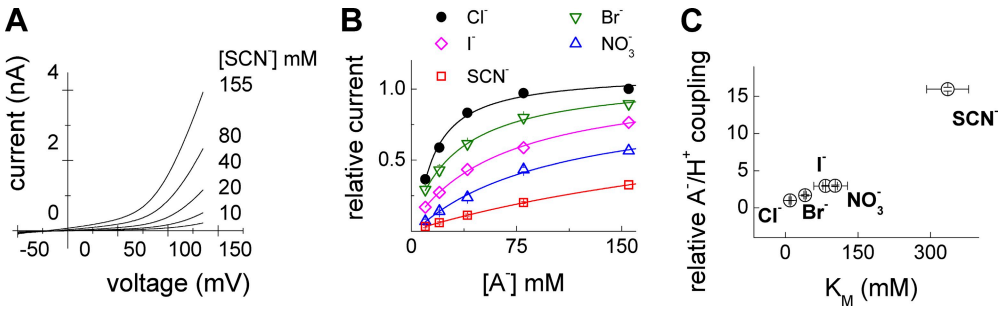

Figure 6. Anion/proton transport stoichiometry of ClC-4 increases with reduced apparent anion binding affinity. (A) Representative current–voltage relationship from a cell perfused with extracellular solutions containing various SCN^- concentrations. Current–voltage relationships were obtained by applying 100-ms voltage ramps from −50 to +135 mV. (B) Dependence of the macroscopic current amplitude at +130 mV on the external anion concentration for various external anions ($n = 4$–7). Lines represent fits with Michaelis-Menten equation to obtain apparent saturation constants. (C) Relative anion/proton coupling as determined in Fig. 1 F plotted against the measured apparent Michaelis constant for various external anions.

mode. To quantify binding of various anions, we measured concentration dependences of ClC-4 current amplitudes (Fig. 6, A and B). Apparent Michaelis constants (K_M) were between 10 ± 2 mM for Cl^- and > 300 mM for SCN^-. These constants are correlated to the apparent anion/proton coupling ratio (Fig. 6 C) and to the ionic radius of the transported anion (Marcus, 1997). Anions with smaller ionic radius occupy a specific binding site for longer time periods and increase the probability of the anion/proton exchange mode.

ClC-4 proton transport is gated by voltage

Scheme 1 predicts that ClC-4 is also voltage gated when functioning as an anion/proton exchanger. Because currents mediated by ClC-4 in the slippage mode might provide a significant fraction of the total current, the observed time and voltage dependence of whole cell currents (Fig. 1) is not sufficient to demonstrate gating of ClC-4 exchangers. Therefore, we performed additional experiments to detect time-dependent changes in proton flux (Fig. 7). In these experiments, rates of intracellular pH changes were determined upon a series of repetitive voltage steps. We varied the duration and frequency of these pulses and determined the effects on intracellular alkanization. Experiments were performed with symmetrical NO_3^- because it increases absolute current amplitudes and only moderately decreases proton flux (Fig. 1), indicating that it supports both transport modes.

Because of its pronounced rectification, ClC-4 proton transport only occurs at positive voltages at an appreciable rate. The time course of pH changes therefore depends on the length of the activating pulses and on the frequency of pulsing. Moreover, effects will be different for transporters that switch between active and not-active forms (gated transporters) than for not-gated transporters. If the number of proton-transporting ClC-4 proteins changes with time and voltage (gated transport), proton currents will activate during voltage steps (Fig. 7 A). In this case, increasing the length of the depolarizing step (T_p) (see top panel in Fig. 7 A) will augment the number of active transporters and thus the rates of intracellular alkalinization (Fig. S5). In contrast, in the case of not-gated transport, the number of proton-transporting ClC-4 proteins will not change with time, and the proton transport rate will not be affected by increased duration of the depolarizing step (T_p), if

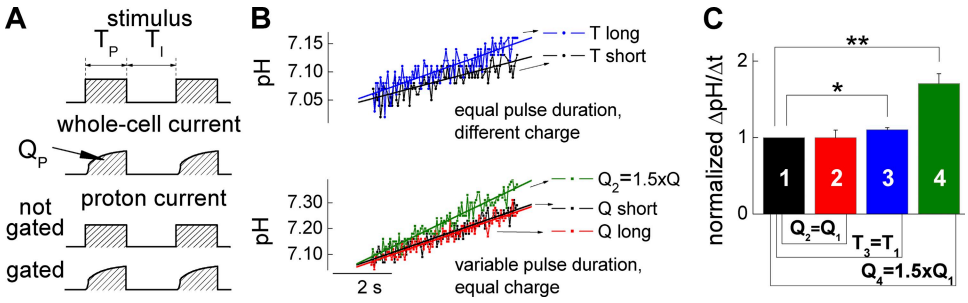

Figure 7. Voltage-dependent gating of ClC-4. (A) Schematic representation of voltage clamp protocols as well as predicted ClC-4 whole cell current and the proton currents for gated and not-gated exchanger function. Voltage steps were repetitively applied with T_P and T_I denoting pulse and interpulse duration. Q_P gives transported charge during a single depolarizing voltage step. (B) Representative intracellular pH recordings from ClC-4–expressing cells stimulated with different voltage protocols. The top panel compares intracellular alkalinization elicited by two protocols with identical total pulse ($\sum T_P$) and total interpulse ($\sum T_I$) durations, $T_P = T_I = 1.5$ *ms* (Tshort) or $T_P = T_I = 3$ *ms* (Tlong), respectively. The bottom panel compares intracellular alkalinization elicited by protocols that differ in total pulse ($\sum T_P$) and total interpulse ($\sum T_I$) durations but exhibit equal total transported charge ($\sum Q_P$). For "Q short," T_P and T_I equal 1.5 ms, whereas "Q long" denotes a pulse protocol with $T_P = 3$ *ms* and $T_I = 3.59$ *ms*. In the protocol "$Q_2 = 1.5$ QT," $T_P = 5$ *ms*, and $T_I = 3.59$ *ms*, resulting in total transported charge, $\sum Q_P$, which is 1.5 times larger compared with pulse protocols "Q short" and "Q long." (C) Statistical analysis of pH responses in several cells ($n = 4$–6).

interpulse duration (T_I) is augmented to the same extent (Fig. 7 A).

For ClC-4, simultaneous doubling of T_p and T_I results in significantly faster rates of intracellular alkalinization (Fig. 7, B, top, and C, column 1 vs. column 3), arguing against time-independent proton transport. As an additional test, we compared proton transport for two pulse protocols in which step and interpulse durations were modified so that the transported charge per time (calculated as the time integral of the measured whole cell current) was the same. The two-pulse protocols resulted in identical intracellular alkalinization rates (Fig. 7, B, bottom, and C, column 1 vs. column 2), suggesting that the time course of total current activation and proton current activation is the same. Modification of pulse and interpulse durations that result in 50% larger transported charge per time increased the rate of pH change by the same degree (Fig. 7, B, bottom, and C, column 1 vs. column 4). All of these experiments demonstrate that proton transport is time and voltage dependent, and that macroscopic proton transport rates change with the same time course as the macroscopic current.

DISCUSSION

We studied transport properties of human ClC-4 heterologously expressed in mammalian cells using ratiometric measurements of intracellular pH, whole cell patch clamp recordings, and noise analysis. We demonstrate that ClC-4 can function as transporter and as channel and switch between the two functional modes depending on the extracellular anion.

Potential interferences of background currents

Mammalian cells express a variety of endogenous currents that might interfere with ClC-4 currents. We performed two different types of experiments to assess the influence of endogenous currents on our experiments. Anion and proton currents were analyzed in untransfected cells as well as in stably transfected cells dialyzed with ATP-free solution. The absence of ATP results in a complete rundown of the ClC-4 currents (Vanoye and George, 2002) with remaining currents that closely resemble currents in untransfected cells. We conclude from these experiments that stable expression of ClC-4 does not result in the up-regulation of endogenous channels. Endogenous currents have much smaller amplitudes than macroscopic ClC-4 currents and therefore only contribute little to macroscopic currents in transfected cells. Moreover, endogenous currents are not associated with proton movements and thus do not interfere with our quantification of ClC-4–mediated proton currents.

Because endogenous channels might have larger single-channel amplitudes than ClC-4, even small background currents could substantially interfere with measurements of ClC-4 current variances. We therefore determined current variances in nontransfected cells (in external SCN^- at +145 mV: 11 ± 2 pA^2; $n = 10$), and these were significantly lower than those in cells expressing functional ClC-4 (see Fig. 3). Moreover, in marked contrast to ClC-4 currents, endogenous currents are virtually time independent. We conclude that endogenous currents do not interfere with noise analysis of ClC-4 currents.

Accuracy of the measured anion/proton coupling rates

Proton fluxes were calculated from time courses of intracellular pH and rely on exact knowledge of two values (buffering capacities and cell volumes) that are difficult to measure accurately. The buffering capacity of the cytoplasm is not constant and depends on the pH. To reduce possible artifacts, we measured cell-buffering capacities individually in every cell and shortened test pulses to avoid large perturbations of cytosolic pH. In addition, we measured and corrected for the pH recovery due to buffer diffusion through the pipette in every cell.

Because the accessibility of closed intracellular compartments for protons is not exactly known, the effective cell volume cannot be accurately determined. This error will lead to an overestimation of effective cell volumes and proton transport rates. For example, if the freely accessible cytosolic volume represented half of the total cell volume, Cl^-/H^+ coupling ratio for Cl^- would be 4:1 instead of 2:1, and unitary proton transport rates in the coupled mode would be only 10^4 s^{-1} at +150 mV. However, this uncertainty does not affect the major conclusion of our paper. An overestimation of the effective cell volume would imply that slippage mode transport rates exceed exchanger transport rates even more than ten-fold, in clear support of distinct underlying transport mechanisms.

Interpretation of noise analysis data

Two earlier studies used nonstationary noise analysis to determine unitary transport rates of ClC-4 (Hebeisen et al., 2003) and ClC-5 (Zdebik et al., 2008). Hebeisen et al. (2003) treated ClC-4 as pure anion channel and obtained unitary current amplitude of 100 fA at +140 mV, slightly above the values reported here for a different anion composition. Zdebik et al. (2008) interpreted noise analysis results on a related isoform, ClC-5, in a completely different way. They assumed that ClC-5 exclusively functions as a transporter and thus generates shot noise. Voltage-dependent gating of transporters and low-pass filtering were proposed to transform shot noise into a Lorentzian type of noise. The use of nonstationary noise analysis let the authors assign unitary transport rates of 10^5 ions/s to coupled exchange by ClC-5.

ClC-4 and ClC-5 are closely similar in primary structure and exhibit the same time and voltage dependence of current amplitudes, indicating that the difference between our results and those of Zdebik et al. (2008) is not

due to isoform-specific functional properties. We disagree with the interpretation of Zdebik et al. (2008) for the following reasons. ClC-4–associated noise largely exceeds the upper limit of shot noise generated by a coupled transporter functioning in a 2:1 stoichiometry given by Schottky's theorem (Fig. 3) (DeFelice, 1981). Our experiments with mixtures of SCN^- and Cl^- (Fig. 5) show that ClC-4 can exist in two modes with different transport rates. Because the variance increases with the square of the current amplitude, even small percentage of slippage mode/channels will significantly contribute to the measured current and variance in external Cl^- and render inaccurate the determination of unitary coupled transport rates by noise analysis. The determined unitary turnover rate of 10^5 ions/s at 100 mV in the exchanger mode (Zdebik et al., 2008) exceeds the maximum transport rates of all currently known coupled transporters. It is one order of magnitude higher than our upper limit of unitary transport rates in the exchanger mode ($\sim 10^4$ at + 100 mV, extrapolated). In addition, it is also two orders of magnitude higher than values obtained from bacterial ClC-ec1 (Walden et al., 2007) and even one order of magnitude higher than the channel mode conductance observed in mutated ClC-ec1 (Jayaram et al., 2008).

The slippage mode of ClC-4 resembles ion channel function

Slippage modes of coupled transporters are characterized by passive transport of only one substrate without coupling to the transport of other substrates (Nelson et al., 2002; DeFelice and Goswami, 2007). Slippage mode has been demonstrated for a variety of transporters; however, the underlying transport mechanisms remained undefined for the majority of these examples. Here, we demonstrate that ClC-4 generates a Lorentzian type of noise under conditions that promote the uncoupled slippage mode (Fig. 3), indicating random switching of unitary current events with amplitudes above the resolution limit. A comparison with simulated data revealed that ClC-4 unitary events have durations between 100 and 200 µs (Fig. 4), largely exceeding values expected for an alternating access mechanism. Moreover, unitary transport rates of ClC-4 in external SCN^- exceed the highest transport rates reported for ion transporters (Brahm, 1977; Hille, 2001). These results define the slippage mode of ClC-4 as a channel type of conduction.

The distribution between ClC-4 being in the exchanger or in the slippage mode depends on the extracellular anion (Figs. 2 and 6). A comparison of the effects of different anions on total currents and proton fluxes revealed a correlation between ionic radius, anion/proton transport stoichiometries, and concentration dependences of current amplitudes (Fig. 6). Assuming that apparent Michaelis constants report the time the anion dwells at a particular position of the ClC-4 pore, these results suggest that a bound anion is required for ClC-4 being in the exchanger mode. Different anions are expected to occupy this site with distinct probabilities depending on their ionic radius. Anions that bind only shortly promote slippage mode behavior with all properties of classical ion channels.

This hypothesis is in agreement with various earlier findings on the bacterial transporter, ClC-ec1. In ClC-ec1, anion and proton transport are strictly coupled in Cl^- but uncoupled in larger and polyatomic anions. Crystallographic analysis of ClC-ec1 in $SeCN^-$, an anion with chemical properties similar to SCN^-, revealed that a central binding site of ClC-ec1 is depleted of anion density (Nguitragool and Miller, 2006). Moreover, a crystallographic study investigating the ion-binding properties of the selectivity filter of ClC-ec1 revealed a Cl^- over Br^- binding selectivity (Lobet and Dutzler, 2005). Lastly, apparent Michaelis constants measured here for Cl^- and Br^- are in a good agreement with the binding affinities obtained from calculating binding site occupancies in ClC-ec1 (Lobet and Dutzler, 2005).

One might expect that a dramatic change in transport mechanism requires pronounced structural rearrangements. This is clearly not the case for ClC-ec1 (Nguitragool and Miller, 2006). Various experimental results support a structural similarity of prokaryotic and eukaryotic ClC-s (Estevez et al., 2003; Engh and Maduke, 2005), suggesting that the change in function of ClC-4 reported here also occurs without major changes in structure.

ClC-4 is a functional intermediate between ClC channels and transporters

The prototypic ClC transporter ClC-ec1 mediates Cl^-/H^+ antiport with transport rates of $\sim$4,000 s^{-1} at 0 mV and a 100-fold anion transmembrane concentration gradient (Walden et al., 2007). In contrast, mammalian ClC anion channels can conduct anions with transport rates above 10^6 or 10^7 s^{-1} (Miller, 1982; Pusch et al., 1994; Weinreich and Jentsch, 2001; Scholl et al., 2006). Our results place ClC-4 between these two functional extremes. In the exchanger mode, transport rates are higher than those of the bacterial ClC isoform, whereas unitary current amplitudes of ClC-4 exceed 1 pA at high voltages in the slippage mode, exceeding single-channel amplitudes of some ClC channels.

Ion channel gating is crucial for many physiological processes. For transporters, time- and voltage-dependent transitions from active to non-active states were only demonstrated for transporter-associated channels or transporters functioning in the slippage mode (Mager et al., 1994; Melzer et al., 2003, 2005). Here, we demonstrate that ClC-4 is not only gated by voltage in the slippage mode, but also when functioning in the exchanger mode (Fig. 7). Voltage-dependent activation of ClC-4 occurs at voltages positive to 0 mV, and it appears unlikely that changes of endosomal membrane potential

will result in full activation of ClC-4 transporters or ClC-4 channels. However, the voltage dependence of relative open probabilities is very shallow (Fig. S3), and thus even small changes in voltage dependence can affect the open probability. Moreover, gating of ClC channels is known to depend on pH and the concentrations of permeant anions (Chen and Hwang, 2008; Jentsch, 2008). Such a modulation is also present in ClC-4 (unpublished data), suggesting a role of voltage-dependent gating in the regulation of endosomal pH by cytoplasmic and intra-endosomal ion concentrations.

Implication for ClC channel/transporter function

Our results demonstrate that ClC-4 can assume slippage modes with all properties that were previously thought to be unique properties of ion channels, i.e., high unitary transport rates and voltage-dependent gating. ClC-type anion exchanger can thus function with properties closely similar to ClC channels. Recently, Lisal and Maduke (2008) demonstrated that voltage-dependent gating of a ClC channel from *Torpedo marmorata*, ClC-0, involves the transmembrane movement of protons, suggesting that ClC channels are broken exchangers with conformational states that are leaky for anions. Both results blur the distinction between channels and transporters even further than previously suggested. ClC exchangers exhibit channel properties, and ClC channels transporter-like features. It is tempting to speculate that ClC channels and antiporters might use the same mechanisms of anion transport. Whereas ClC channels exclusively function in the slippage mode, transporters are also capable to mediate thermodynamically coupled exchange.

Lisal and Maduke (2008) identified one particular step, i.e., the transport of H^+ from the internal to the external membrane site as necessary for voltage-dependent gating in ClC-0. Assuming that similar conformational changes trigger the gating of ClC-0 and ClC-4, our finding that ClC-4 exhibits voltage-dependent gating in its exchanger as well as in its channel mode suggests that anion-dependent uncoupling does not affect partial reaction steps underlying H^+ transport.

Physiological impact

In endosomes, ClC-3 to ClC-7 are believed to act in conjunction with primary active proton transporters to ensure electrical neutrality of proton movement into cell compartments (Gunther et al., 1998; Iyer et al., 2002). Such function can be fulfilled by anion channels as well as by anion–proton exchangers (Faundez and Hartzell, 2004). With Cl^- as a main permeant anion, ClC transporters appear to function exclusively as coupled exchangers (Accardi and Miller, 2004; Graves et al., 2008). However, anions that were shown to uncouple ClC-type transporters are present in the human body. Because of the different turnover rates of exchanger and slippage modes, even low concentrations of these anions might have significant effects on anion current amplitudes. 1% of the total number of transporters in the slippage mode will result in 10% anion transport uncoupled to proton movements. ClC-5 was recently demonstrated to actively participate in the control of iodide metabolism (van den Hove et al., 2006). Variations in iodide concentrations will lead to variable ClC-5 transport coupling and modulate iodide uptake. Similar mechanisms may be involved in the metabolism of nitrate and nitrite, anions with emerging physiological importance (Lundberg et al., 2008).

Anion channels and coupled Cl^-/H^+ antiporters have different equilibrium potentials (Accardi and Miller, 2004). These thermodynamic differences can result in inward anion currents mediated by ClC exchangers and outward anion currents mediated by ClC channels under certain conditions. Depending on its transport mode, a fraction of ClC-4 will thus exert different effects on endosomal acidification than the remaining ones. Here, we demonstrated that extracellular and correspondingly intra-endosomal anions affect the relative number of ClC-4 exchangers and channels. Other physiological factors, such as pH, or yet to be defined regulatory pathways and accessory subunits might have similar effects and regulate endosomal pH by modulating the transport mode of ClC exchangers (Alekov and Fahlke, 2008).

We would like to thank Drs. Patricia Hidalgo and Martin Fischer for helpful discussions.

These studies were supported by the Deutsche Forschungsgemeinschaft (FOR450, TP10 to C. Fahlke).

Paul J. DeWeer served as editor.

Submitted: 11 November 2008
Accepted: 26 March 2009

REFERENCES

Accardi, A., and C. Miller. 2004. Secondary active transport mediated by a prokaryotic homologue of ClC Cl^- channels. *Nature.* 427:803–807.

Accardi, A., M. Walden, W. Nguitragool, H. Jayaram, C. Williams, and C. Miller. 2005. Separate ion pathways in a Cl^-/H^+ exchanger. *J. Gen. Physiol.* 126:563–570.

Accardi, A., S. Lobet, C. Williams, C. Miller, and R. Dutzler. 2006. Synergism between halide binding and proton transport in a CLC-type exchanger. *J. Mol. Biol.* 362:691–699.

Alekov, A.K., and C. Fahlke. 2008. Anion channels: regulation of ClC-3 by an orphan second messenger. *Curr. Biol.* 18:R1061–R1064.

Barry, P.H. 1994. JPCalc, a software package for calculating liquid junction potential corrections in patch-clamp, intracellular, epithelial and bilayer measurements and for correcting junction potential measurements. *J. Neurosci. Methods.* 51:107–116.

Brahm, J. 1977. Temperature-dependent changes of chloride transport kinetics in human red cells. *J. Gen. Physiol.* 70:283–306.

Chen, T.Y., and T.C. Hwang. 2008. CLC-0 and CFTR: chloride channels evolved from transporters. *Physiol. Rev.* 88:351–387.

Chen, T.Y., and C. Miller. 1996. Nonequilibrium gating and voltage dependence of the ClC-0 Cl^- channel. *J. Gen. Physiol.* 108:237–250.

De Angeli, A., D. Monachello, G. Ephritikhine, J.M. Frachisse, S. Thomine, F. Gambale, and H. Barbier-Brygoo. 2006. The nitrate/proton antiporter AtCLCa mediates nitrate accumulation in plant vacuoles. *Nature.* 442:939–942.

DeFelice, L.J. 1981. Introduction to Membrane Noise. Plenum Press, New York. 500 pp.

DeFelice, L.J., and T. Goswami. 2007. Transporters as channels. *Annu. Rev. Physiol.* 69:87–112.

Engh, A.M., and M. Maduke. 2005. Cysteine accessibility in ClC-0 supports conservation of the ClC intracellular vestibule. *J. Gen. Physiol.* 125:601–617.

Estevez, R., B.C. Schroeder, A. Accardi, T.J. Jentsch, and M. Pusch. 2003. Conservation of chloride channel structure revealed by an inhibitor binding site in ClC-1. *Neuron.* 38:47–59.

Faundez, V., and H.C. Hartzell. 2004. Intracellular chloride channels: determinants of function in the endosomal pathway. *Sci. STKE.* 2004:re8.

Galli, A., C.I. Petersen, M. deBlaquiere, R.D. Blakely, and L.J. DeFelice. 1997. Drosophila serotonin transporters have voltage-dependent uptake coupled to a serotonin-gated ion channel. *J. Neurosci.* 17:3401–3411.

Graves, A.R., P.K. Curran, C.L. Smith, and J.A. Mindell. 2008. The Cl^-/H^+ antiporter ClC-7 is the primary chloride permeation pathway in lysosomes. *Nature.* 453:788–792.

Gunther, W., A. Luchow, F. Cluzeaud, A. Vandewalle, and T.J. Jentsch. 1998. ClC-5, the chloride channel mutated in Dent's disease, colocalizes with the proton pump in endocytotically active kidney cells. *Proc. Natl. Acad. Sci. USA.* 95:8075–8080.

Hamill, O.P., A. Marty, E. Neher, B. Sakmann, and F.J. Sigworth. 1981. Improved patch-clamp techniques for high-resolution current recording from cells and cell-free membrane patches. *Pflugers Arch.* 391:85–100.

Hebeisen, S., L. Heidtmann, D. Cosmelli, C. Gonzalez, B. Poser, R. Latorre, O. Alvarez, and Ch. Fahlke. 2003. Anion permeation in human ClC-4 channels. *Biophys. J.* 84:2306–2318.

Heinemann, S.H., and F. Conti. 1992. Nonstationary noise analysis and application to patch clamp recordings. *Methods Enzymol.* 207:131–148.

Hille, B. 2001. Ionic Channels of Excitable Membranes. 3rd ed. Sinauer Associates Inc., Sunderland, MA. 814 pp.

Iyer, R., T.M. Iverson, A. Accardi, and C. Miller. 2002. A biological role for prokaryotic ClC chloride channels. *Nature.* 419:715–718.

Jardetzky, O. 1966. Simple allosteric model for membrane pumps. *Nature.* 211:969–970.

Jayaram, H., A. Accardi, F. Wu, C. Williams, and C. Miller. 2008. Ion permeation through a Cl^--selective channel designed from a CLC Cl^-/H^+ exchanger. *Proc. Natl. Acad. Sci. USA.* 105:11194–11199.

Jentsch, T.J. 2008. CLC chloride channels and transporters: from genes to protein structure, pathology and physiology. *Crit. Rev. Biochem. Mol. Biol.* 43:3–36.

Kolb, H.A., and P. Läuger. 1978. Spectral analysis of current noise generated by carrier-mediated ion transport. *J. Membr. Biol.* 41:167–187.

Lang, K., C. Wagner, G. Haddad, O. Burnekova, and J. Geibel. 2003. Intracellular pH activates membrane-bound Na^+/H^+ exchanger and vacuolar H^+-ATPase in human embryonic kidney (HEK) cells. *Cell. Physiol. Biochem.* 13:257–262.

Lisal, J., and M. Maduke. 2008. The ClC-0 chloride channel is a 'broken' Cl^-/H^+ antiporter. *Nat. Struct. Mol. Biol.* 15:805–810.

Lobet, S., and R. Dutzler. 2005. Ion-binding properties of the ClC chloride selectivity filter. *EMBO J.* 25:24–33.

Lundberg, J.O., E. Weitzberg, and M.T. Gladwin. 2008. The nitrate-nitrite-nitric oxide pathway in physiology and therapeutics. *Nat. Rev. Drug Discov.* 7:156–167.

Mager, S., C. Min, D.J. Henry, C. Chavkin, B.J. Hoffman, N. Davidson, and H.A. Lester. 1994. Conducting states of a mammalian serotonin transporter. *Neuron.* 12:845–859.

Marcus, Y. 1997. Ion Properties. CRC Press. 272 pp.

Mathias, R.T., I.S. Cohen, and C. Oliva. 1990. Limitations of the whole cell patch clamp technique in the control of intracellular concentrations. *Biophys. J.* 58:759–770.

Matsuda, J.J., M.S. Filali, K.A. Volk, M.M. Collins, J.G. Moreland, and F.S. Lamb. 2008. Overexpression of CLC-3 in HEK293T cells yields novel currents that are pH dependent. *Am. J. Physiol. Cell Physiol.* 294:C251–C262.

Melzer, N., A. Biela, and Ch. Fahlke. 2003. Glutamate modifies ion conduction and voltage-dependent gating of excitatory amino acid transporter-associated anion channels. *J. Biol. Chem.* 278:50112–50119.

Melzer, N., D. Torres-Salazar, and Ch. Fahlke. 2005. A dynamic switch between inhibitory and excitatory currents in a neuronal glutamate transporter. *Proc. Natl. Acad. Sci. USA.* 102:19214–19218.

Miller, C. 1982. Open-state substructure of single chloride channels from *Torpedo* electroplax. *Philos. Trans. R. Soc. Lond. B Biol. Sci.* 299:401–411.

Nelson, N., A. Sacher, and H. Nelson. 2002. The significance of molecular slips in transport systems. *Nat. Rev. Mol. Cell Biol.* 3:876–881.

Nguitragool, W., and C. Miller. 2006. Uncoupling of a CLC Cl^-/H^+ exchange transporter by polyatomic anions. *J. Mol. Biol.* 362:682–690.

Picollo, A., and M. Pusch. 2005. Chloride/proton antiporter activity of mammalian CLC proteins ClC-4 and ClC-5. *Nature.* 436:420–423.

Pusch, M., K. Steinmeyer, and T.J. Jentsch. 1994. Low single channel conductance of the major skeletal muscle chloride channel, ClC-1. *Biophys. J.* 66:149–152.

Roos, A., and W.F. Boron. 1981. Intracellular pH. *Physiol. Rev.* 61:296–434.

Scheel, O., A.A. Zdebik, S. Lourdel, and T.J. Jentsch. 2005. Voltage-dependent electrogenic chloride/proton exchange by endosomal CLC proteins. *Nature.* 436:424–427.

Scholl, U., S. Hebeisen, A.G. Janssen, G. Muller-Newen, A. Alekov, and Ch. Fahlke. 2006. Barttin modulates trafficking and function of ClC-K channels. *Proc. Natl. Acad. Sci. USA.* 103:11411–11416.

Sigworth, F.J. 1980. The variance of sodium current fluctuations at the node of Ranvier. *J. Physiol.* 307:97–129.

Silberberg, S.D., and K.L. Magleby. 1993. Preventing errors when estimating single channel properties from the analysis of current fluctuations. *Biophys. J.* 65:1570–1584.

Starace, D.M., and F. Bezanilla. 2004. A proton pore in a potassium channel voltage sensor reveals a focused electric field. *Nature.* 427:548–553.

Stevens, C.F. 1972. Inferences about membrane properties from electrical noise measurements. *Biophys. J.* 12:1028–1047.

van den Hove, M.F., K. Croizet-Berger, F. Jouret, S.E. Guggino, W.B. Guggino, O. Devuyst, and P.J. Courtoy. 2006. The loss of the chloride channel, ClC-5, delays apical iodide efflux and induces a euthyroid goiter in the mouse thyroid gland. *Endocrinology.* 147:1287–1296.

Vanoye, C.G., and A.L. George Jr. 2002. Functional characterization of recombinant human ClC-4 chloride channels in cultured mammalian cells. *J. Physiol.* 539:373–383.

Verveen, A.A., and L.J. DeFelice. 1974. Membrane noise. *Prog. Biophys. Mol. Biol.* 28:189–265.

Walden, M., A. Accardi, F. Wu, C. Xu, C. Williams, and C. Miller. 2007. Uncoupling and turnover in a Cl^-/H^+ exchange transporter. *J. Gen. Physiol.* 129:317–329.

Weinreich, F., and T.J. Jentsch. 2001. Pores formed by single subunits in mixed dimers of different CLC chloride channels. *J. Biol. Chem.* 276:2347–2353.

Zdebik, A.A., G. Zifarelli, E.Y. Bergsdorf, P. Soliani, O. Scheel, T.J. Jentsch, and M. Pusch. 2008. Determinants of anion-proton coupling in mammalian endosomal CLC proteins. *J. Biol. Chem.* 283:4219–4227.